American Mineralogist, Volume 67, pages 1101–1117, 1982

On the mechanism of contact aureole formation in dolomitic country rock by the Adamello intrusion (northern Italy)

KURT BUCHER-NURMINEN

Mineralogisches Institut der Universität Basel
Bernoullistr. 30, 4056 Basel, Switzerland

Abstract

Intrusion of the Adamello granite (Tertiary) in the southern Alps (northern Italy) caused a distinct mineralogical and chemical zonation within the country rock dolomites. The contact aureole can be divided into an inner aureole characterized by the widespread and abundant occurrence of forsterite and spinel (±clinohumite); and an outer aureole with widespread but modally subordinate tremolite. The forsterite isograde separating the two zones is a clear, mappable boundary in the field. The mineralogical changes across the isograd are accompanied by a significant increase of modal silicate and oxide minerals towards the forsterite zone. Open pore spaces and cavities in dolomite of the outer aureole are progressively sealed with silicate + oxide assemblages towards the contact, resulting in a nodular, silicate-rich marble.

It is concluded that the observed zonation may have resulted from infiltration and reaction of silica- and alumina-rich fluids, given off by the cooling pluton within the dolomitic country rock. This conclusion is further supported by the microtextures of many of the forsterite-zone samples. The geochemical model proposed for the mechanism of aureole formation suggests that SiO_2 dissolved in the inferred fluid was filtered out by a reaction of the type $2Do + SiO_{2aq} = Fo + 2Cc + 2CO_2$. Samples from roof pendants show evidence that CaO was not conserved in the above reaction, rather that calcite dissolved congruently and was partially removed from the site of reaction. The forsterite isograd is interpreted as the main infiltration front during the formation of the metasomatic aureole.

Introduction

Various effects of high level igneous intrusions on carbonate country rocks have been discussed in a number of recently published field studies. It has been demonstrated in a number of cases that the observed zonation of the aureole may be attributed to thermal metamorphism (Kerrick, 1970, Rice, 1977, Masch, 1977, Melson, 1966). The composition of the inferred metamorphic fluid has been shown to be controlled by the local mineral assemblage throughout the aureole. Prograde metamorphism occurred along a definite "buffer path" (Greenwood, 1975), given by the initial bulk composition of the carbonate rock and thermal regime of the aureole. In a number of other field examples it has been shown that the buffer capacity of the local assemblages was partially or completely exhausted by the introduction of H_2O from the pluton. H_2O-metasomatism in addition to the thermal effect of the intrusion was seen as a major control of the mineralogical zonation of the aureole (Moore and Kerrick, 1976, Suzuki, 1977). Other effects of chemical transport include the formation of skarns (*i.e.*, Taylor and O'Neil, 1977) and hydrothermal vein formation (Bucher, 1981a).

The present study describes a contact aureole in dolomitic country rocks from the southern Alps. The data from this particular field example suggest that the observed mineralogical zoning of the aureole is the result of SiO_2-metasomatism along steep temperature gradients imposed by the pluton.

General geology

The Adamello pluton is the largest Tertiary intrusion in the Alps and is located north of Brescia (northern Italy). The pluton is a composite intrusion consisting of interfingered stocks of granite and granodiorite together with at least two types of tonalite. Numerous small bodies of diorite, gabbro and gabbro–diorite occur along the contact zone (Bianci and Dal Piaz, 1948). The whole pluton measures some 60 km in length while the width is

0003–004X/82/1112–1101$02.00

between 7 km and 22 km. The pluton intrudes pre-Permian crystalline basement rocks in the north and Permian and Mesozoic sediments in the south. In the area of Cima Uzza (southeast rim of the intrusion) the intrusives are in contact with Mesozoic dolomitic sediments (Callegary, 1962). Two profiles have been studied in detail: (1) a profile at Cima di Agosta and (2) from Cima Uzza to the south (Fig. 1). This second profile is characterized by intrusive rocks with numerous small carbonate roof pendants near the summit of Cima Uzza, while south of the passo del Frato (Fig. 1), non-dolomitic sediments are intercalated in the low-grade part of the aureole. The dolomitic sediments belong to the Esino Formation of Triassic age (Ladin) and are either pure dolomites or dolomitic limestones (Callegary, 1962).

Apart from massive pure dolomite, well stratified dolomitic limestones sequences occur in the formation as well as brecciated marbles. In the outer aureole, the dolomites are frequently very porous with cavities typically 1 to 2 mm in diameter (maximum cavity size 3 cm).

Figure 1a shows a cut surface of sample Ca 196. The rock is generally very porous and the cavities can measure up to 2 cm in diameter. The pore space in many instances is interconnected in a three-dimensional network. The cavities are frequently coated with tremolite. In sample Ca 196 talc is also present as a wall coating. The matrix rock is an extremely pure dolomite–calcite marble. Note that the rock is cut by numerous veinlets (three visible on the surface shown in Fig. 1a). These veinlets are filled by white calcite, although some lenticular open spaces may still be present along the veinlets. These veinlets may represent the pathways for hydrothermal fluids to pass through the country rock and may have also connected larger primary

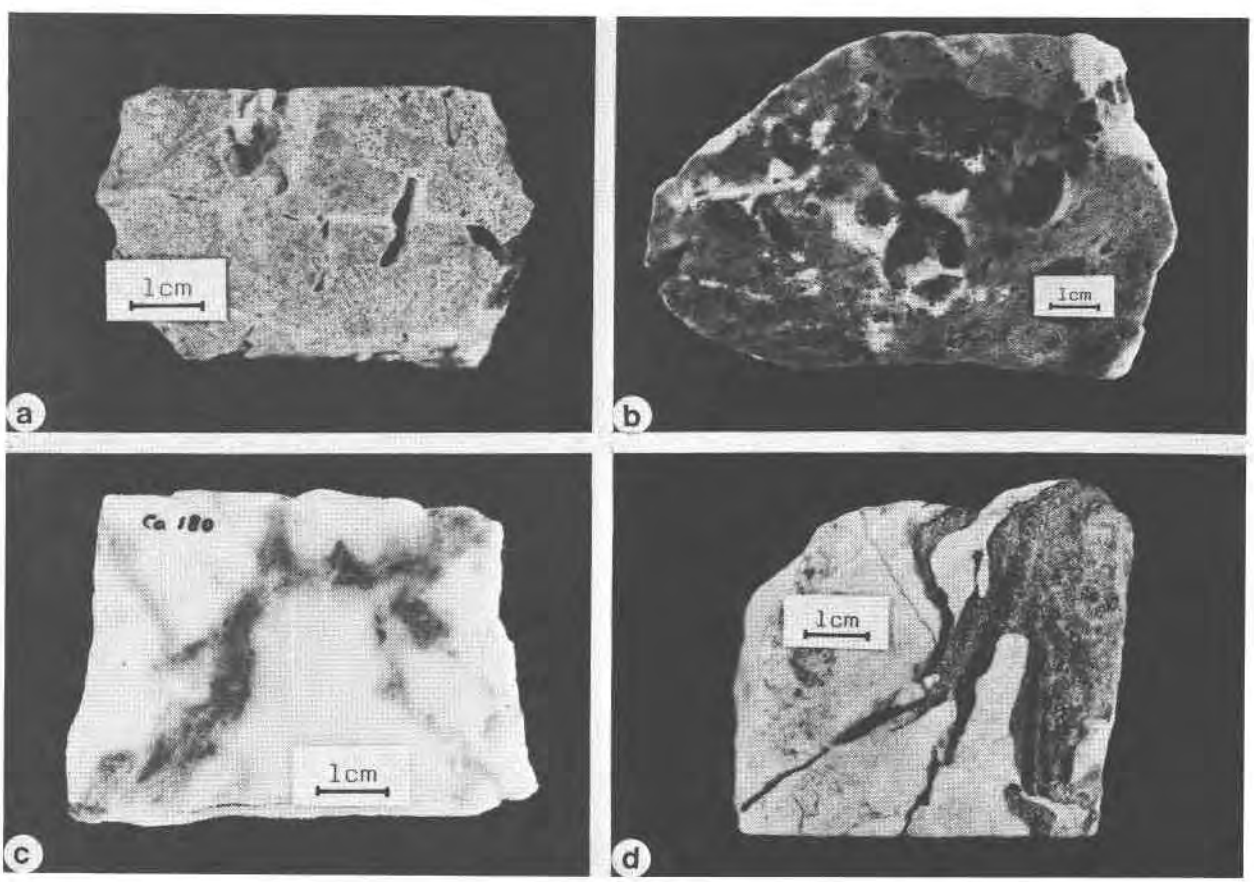

Fig. 1. Photographs of dolomitic marbles from the profile at Cima Uzza. (a) Sample Ca196: porous dolomite from the outer aureole; (b) Sample Ca185: nodular spinel–forsterite–marble; (c) Sample Ca180: veinlets of spinel–forsterite–clinohumite–marble in pure dolomite matrix; and (d) Sample Ca180: weathered surface with larger irregular nodules rich in silicate minerals surrounded by pure dolomitic marble.

cavities, making them accessible to the presumed fluid. The deposition of tremolite and other silicate minerals along the cavity walls and within the veinlets suggests that the pore space was probably primary and unlikely to be the result of postmetamorphic dissolution and removal of silicate nodules or siliceous fossils. Furthermore, it should be noted that siliceous nodules or siliceous fossils have not been found in unmetamorphosed Esino dolomites. The pore space of porous dolomite is progressively reduced towards its contact with the Adamello intrusion.

The inner aureole is defined by the first appearance of forsterite. Many of the marbles display nodular regions composed of forsterite–spinel–clinohumite–calcite. These nodules are interpreted as filling former open cavities. Figure 1b shows the weathered surface of sample Ca 185 with its characteristic nodular texture. The nodules are very rich in silicate, oxide and sulfide minerals, whereas the matrix of the rock is pure dolomite with rare minute flakes of phlogopite. The bulk composition of the matrix is equivalent to that of the marbles of the outer aureole. Figures 1c and 1d show the textural relationships on a cut and a fresh surface of sample Ca 180 respectively. In this example, the minerals of the assemblage forsterite–clinohumite–spinel–calcite are all in contact with the dolomite of the matrix, and some retrograde (?) chlorite. These phases are concentrated in irregular nodules which are also interconnected by veins of complex geometry. The same minerals are found in the veins as in the nodules. The matrix rock is again a very pure, coarse grained dolomitic marble. The texture of the weathered surface (Fig. 1d) suggests that the silicate rich nodules are of metasomatic origin. The pure dolomite "finger" on the surface is suggestive of a residual dolomite domain resulting from the incomplete reaction between matrix dolomite and inferred fluid phase.

The forsterite zone samples not affected by metasomatism have similar bulk rock composition compared to the unmetamorphosed rocks. Their mineralogy is characterized by a coarse dolomite matrix with scarce, isolated grains of forsterite, spinel, clinohumite and phlogopite. The modal abundance of non-carbonate minerals is on the order of 1%.

Relative increase of the silicate minerals due to carbonate breakdown and volume reduction cannot account for the magnitude of systematic increase of silicate and oxide minerals beyond the forsterite isograd.

The lithological characteristics of the rocks examined are summarized in Table 1b. The rock type (A) corresponds to "marmo dolomitico saccaroide" and "marmoi calcareo–dolomitici saccaroide" in the terminology of Callegary (1962). Except for the very rare quartzitic and marly layers, the bulk of the carbonate sediments are extremely poor in non-carbonate minerals. The silicate minerals in many of the samples from the outer aureole were determined by X-ray diffraction techniques from residues prepared by dissolution of the carbonates in cold acetic acid.

Callegary (1962) presented a number of bulk rock analyses of (A)-type marble ("marmo dolomitico saccaroide", Callegary, 1962: Table 4). He found that unmetamorphic rocks and tremolite zone marbles had insoluble residues (non-carbonate minerals) typically about 1% or less. Metasomatized marbles from the forsterite zone, corresponding to the nodular silicate-rich rocks (Fig. 1b and 1c) may have residues as high as 40%. Unmetasomatized marbles from the forsterite zone revealed compositions similar to those of the low grade portions of the aureole. Figure 2 shows the estimated *maximum* modal abundance of non-carbonate minerals in the Cima Uzza profile. In this context maximum modal abundance means the modal abundance of non-carbonate minerals in the typically silica-rich nodules such as those shown in Figures 1b, 1c and 1d. Such silicate-rich nodules are unknown from the lower grade portions of the aureole. The term metasomatized marble introduced above refers to the nodular marbles of the forsterite zone and to the porous tremolite rocks from the outer aureole and follows from the interpretation of macroscopic rock textures. The term does not refer to the skarn rocks

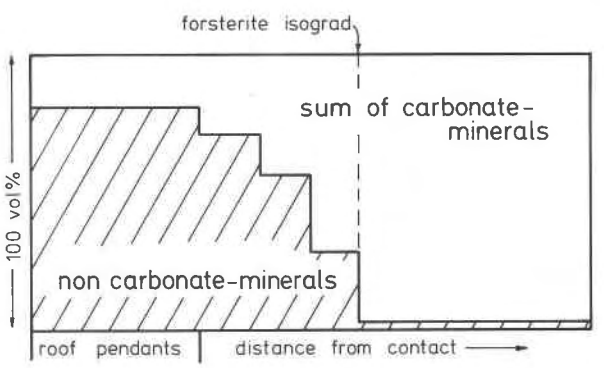

Fig. 2. *Maximum* modal content of non-carbonate minerals found in marble samples as a function of distance from the contact to the intrusion. Note that inside the forsterite zone, many of the marbles are still pure dolomites.

found at the immediate contact to the intrusives. Xanthophyllite–garnet–fassaite–spinel skarns, along with other types are described by Callegary (1962). The usage of the term "metasomatic" here is consistent with Callegary (1962), who has suggested that many of the marbles rich in silicate and oxide minerals may have formed by metasomatism. His conclusion was not restricted to clearly metaso-

Table 1. Observed mineral assemblages listed in the order of increasing distance from the intrusion. Abbreviations are given on Table 1a. For the definition of rock types see Table 1b.

sample number	carbonates	olivine clinohumite	amphibole talc	chlorite spinel	micas	other minerals	opaque minerals	retrogr. minerals	rock type
169*	CC+DO	FO+CLH							A
170*	CC+DO	FO+CLH		SP	PHL		PY+GAL		C
171*	CC+DO	FO+CLH		SP			PY	TR	A
172*	CC+DO	FO+CLH		SP			PY+PEN		B
173	CC+DO	FO							A
174	CC+DO	FO		SP				DO+CHL	D
175	CC+DO	FO		SP				CHL	E
176	CC	FO+CLH		SP				CHL	E
177*	CC+DO	FO			PHL			CHL+TR	
178*	CC+DO	CLH		SP				CHL	A
179	CC+DO					BR			A
180	CC+DO	FO+CLH		SP+CHL				CHL	A
181	CC	FO		SP				CHL	E
182	CC	FO		SP				CHL	E
184*	CC+DO	FO+CLH	AM	SP+CHL			PY+MT+GA		A
185*	CC+DO	FO+CLH	AM	CHL			PR+ST+GA		A
186*	CC+DO	FO+CLH	AM	SP+CHL		AP	PY+MT+GA	TR	A
187*	CC+DO	FO		SP+CHL	PHL		PY+RU		A
188	CC+DO	FO	AM			ANT		ANT	E
189*	CC+DO	FO+CLH	AM				MT	TR	A
190	CC+DO		AM	CHL	PHL	ANT			A
206	CC+DO				PHL				A
205	CC+DO		AM						A
204	CC+DO		AM			ANT			A
203	CC				PHL+MU		PY		F
202	CC+DO		AM	CHL	MU	QZ			A
201	CC				MU	PKL			D
200	CC+DO		AM+TC						D
198	CC+DO			CHL	MU	QZ			A
197	CC+DO		AM+TC	CHL	MU				D
196*	CC+DO		AM+TC	CHL	PHL+MU		PY+GA		A
195	CC+DO				MU				A
194	CC+DO								A
193	CC+DO			CHL	MU	KFS+PKL+QZ			A
192	CC+DO				MU	PKL			A
191	CC+DO				MU	KFS+QZ	PY+HE		A
207	CC+DO		AM	CHL	MU				A
208	CC+DO		AM		MU	ANT			A
209	CC+DO			CHL	MU				A
212	CC+DO	FO							A
213*	CC+DO	FO+CLH	AM	SP	PHL	DI	RU+PY+GA	DO+CHL	D
214*	CC+DO	FO		SP	PHL			CHL	A
215	CC+DO	FO		SP	PHL			DO	E
216*	CC+DO	FO		SP	PHL		IL+MT+PR	ANT	D
217	CC+DO	FO+CLH	AM	SP	PHL			DO+CHL	D
218	CC+DO	FO		SP				DO+CHL+TR	D
219	CC	FO		SP	PHL	DI+XA		DO+CHL	E
220	CC+DO	FO+CLH		SP				CHL	D
210*	CC+DO	FO	AM				PY+PR		C
211*	CC+DO	FO+CLH	AM	SP+CHL	PHL		PY+MT+GA		C

*denotes microprobe samples (opaque minerals were determined on probe samples only)

Table 1a. Abbreviations of mineral names

AM	amphibole	MU	muscovite
ANT	antigorite	MT	magnetite
AP	apatite	PEN	pentlandite
BR	brucite	PHL	phlogopite
CC	calcite	PKL	plagioclase
CHL	chlorite	PR	pyrite
CLH	clinohumite	PY	pyrrotite
DI	diopside	QZ	quartz
DO	dolomite	RU	rutile
FO	forsterite	SP	spinel
GA	galenite	ST	sphalerite
HE	hematite	TC	talc
IL	ilmenite	TR	tremolite
KFS	K-feldspar	XA	xanthophyllite

matic scarns at the immediate contacts but also included many of the nodular dolomitic marbles of the forsterite zone as well.

Mineralogical zonation

The mineral assemblages found in the aureole are listed in Table 1, in order of increasing distance from the intrusive contact. Samples 169 through 177 have been collected from roof pendants enclosed in the intrusive rocks. Samples 178 through 196 represent a continuous profile from the contact to the outer portion of the aureole. Samples 207–209 were collected on the eastern flank of Cima Uzza, whereas samples 195–191 are from the "non-metamorphosed" dolomites south of Passo del Frato. Samples 210–220 have been collected from a parallel profile at Cima di Agosta, east of Cima Uzza.

A clear, systematic mineralogical zonation is evident (Table 1) and the areal distribution of mineral assemblages in the system CaO–MgO–Al_2O_3–SiO_2–CO_2–H_2O is presented in Figure 3. The typical assemblage in the unmetamorphic part of the aureole is dolomite + calcite + quartz + chlorite. Just north of the outcrop gap, in the low grade portion of the aureole, talc and tremolite are present in the marbles, however, the paucity of talc-bearing samples precludes the location of a "talc out" isograd. The only isograd which could be mapped was found to be the first appearance of the forsterite (shown as dashed line labeled "3", Fig. 3). The outer aureole is consequently referred to as the tremolite zone, the inner aureole as the forsterite zone. Some general features of the two zones and the separating forsterite–isograd are outlined below.

Table 1b. Definition of rock types

A) The matrix of the rock is a very pure calcite-dolomite marble,
inner aureole: nodules rich in non carbonate minerals,
outer aureole: open cavities or brecciated texture,

B) The matrix of the rock is a pure dolomite, contains very large (> 10cm) silicate-rich nodules,

C) Banded silicate-rich marble,

D) Finely banded silicate-poor marble,

E) Patchy silicate-rich calcite marble (partly with silicate veins or other evidence of metasomatism),

F) Dense pure calcite marble,

Outer aureole (tremolite zone)

Talc occurs as minute flakes (<0.5 mm) in the outer portion of the tremolite zone. The textures involving talc are difficult to interpret. Parallel intergrowth with tremolite and even replacement of tremolite by talc were observed. However, talc is clearly restricted to the outermost portion of the aureole. Quartz-bearing samples, widespread in the outermost aureole and in nonmetamorphic dolomites, persist distinctly closer to the contact than talc-bearing dolomites. Antigorite was detected in a

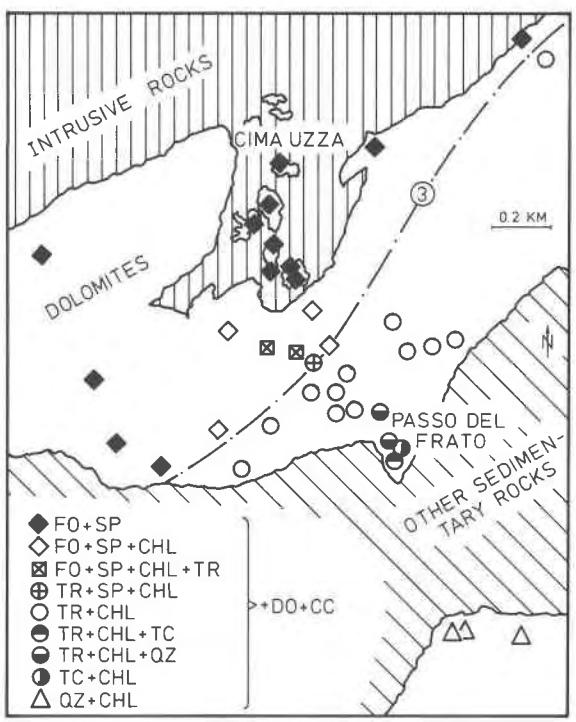

Fig. 3. Distribution of mineral assemblages along the profile from Cima Uzza. The dashed line labeled 3 represents the forsterite isograd.

number of samples from the tremolite zone. This serpentine mineral occurs on fracture surfaces or together with tremolite in veinlets. It could be interpreted from the textures of antigorite-bearing samples that this mineral is of late (retrograde ?) origin and does not represent a prograde mineral phase. However, it must be noted that the occurrence is restricted to the tremolite-zone. The zonal distribution of ophidolomite in the aureole is consistent with a prograde interpretation of the antigorite assemblages. Phlogopite and chlorite are present throughout the tremolite zone, whereas muscovite disappears prior to the first appearance of forsterite. The disappearance of muscovite could not be mapped as an isograd.

The forsterite isograd

The isograd is a distinct and mappable boundary in the field. It is characterized by the abrupt and abundant appearance of coarse grained forsterite and coincides with the first appearance of clinohumite and spinel.

The inner aureole (forsterite zone)

Forsterite represents the predominant silicate mineral within this zone. It is commonly accompanied by clinohumite and spinel. Amphibole disappears from the assemblages clearly inside the forsterite zone. Textures of chlorite are commonly ambiguous and the distinction of prograde growth as opposed to late secondary chlorite growth may be obscure. However, prograde chlorite probably remains in the rocks beyond the "amphibole-out" boundary. Brucite-marbles are comparatively rare in the aureole and only one sample is listed in Table 1. However, Callegary (1962) described brucite marbles from the Uzza areas as well. One sample contains the assemblage calcite–dolomite–brucite. This essentially silica-free rock is similar to Cc 179. Another sample of brucite marble described by Callegary (1962) contains the assemblage calcite–dolomite–brucite–forsterite–spinel. Brucite occurs in the characteristic pseudomorph texture after periclase (?). Diopside does not occur in the samples of the Cima Uzza profile. This pyroxene has been found in samples from the Agosta-profile where it coexists with dolomite, amphibole and forsterite.

Mineral reactions and isograds

The systematic succession of observed mineral assemblages as shown in Figures 3 and 4 and listed in Table 1 may be related to a sequence of successive mineral reactions linking the different assemblages. The equilibrium conditions of these reactions in terms of the variables T and X_{CO_2} at constant P[1] are shown on Figure 5 for the system CaO–MgO–SiO_2–CO_2–H_2O. On Figure 6 a number of additional relevant equilibria are shown in addition to the equilibria presented on Figure 5.

All phase diagrams (Figs. 5, 6, 11 and 12) were calculated making use of the programs REACTION (Finger and Burt, 171), SUPCRT (Helgeson and others, 1978) and FINDX (Flowers, 1978) utilizing the thermodynamic data given by Helgeson and others (1978) and Walther and Helgeson (1977). The data for clinochlore were slightly adjusted in order to be consistent with data of Widmark (1980) and Fawcett and Yoder (1966). The following standard states were used in all calculations: for solids and gases unit activity of the pure compounds at P and T. For aqueous species: unit activity of the species in a hypothetical 1 molal solution referenced to infinite dilution at P and T. Ideal mixing of CO_2 and H_2O was assumed (*i.e.*, $a_{H_2O} = X_{H_2O}$) ignoring the effect of dissolved species other than CO_2. The composi-

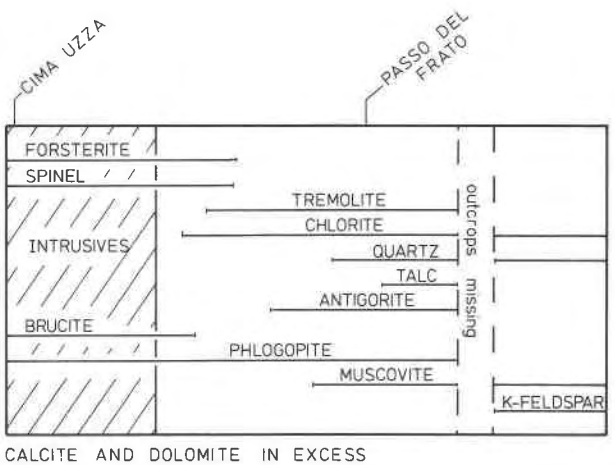

Fig. 4. Distribution of minerals in calcite–dolomite marbles of the Cima Uzza area.

[1]All phase diagrams were calculated for P = 1 kbar Stratigraphic evidence (Callegary 1962), the occurrence of extremely fine grained hornfelses in the area as well as the preserved open pore spaces in the dolomites suggest that load pressure was probably low. On the other hand the occurrence of the assemblage calcite + dolomite + antigorite + tremolite requires pressures above 750 bars, the inversion pressure for the two alternative topologies for ophicarbonate equilibria (Trommsdorff and Evans, 1977).

tion of the fluid phase was approximated by $P_{CO_2} + P_{H_2O} = P_t$. The solvation of the aqueous species is formally taken into account employing the σ-notation according to Walther and Helgeson (1980).

All phase diagrams were calculated for pure endmember components (compositions defined by Helgeson and others, 1978). Displacements of the equilibrium conditions could result from the presence of complex solid solutions rather than endmembers in the natural samples. However, Rice (1977) and Bucher (1981b) presented estimates on the magnitude of this effect from the same rock types and comparable mineral compositions. They concluded that the displacement of the equilibrium curves of Figures 5 and 6 due to solid solution is not likely to exceed ±10°. This assumption is probably applicable to this study as well, because the compositions of the minerals of the Adamello aureole are generally closer to the endmember compositions than those reported in Rice (1977) and Bucher (1981b).

The following discussion refers to Figure 4 and will proceed from the right (south, unmetamorphic) side to the left (north, roof pendants). The disappearance of K-feldspar and the appearance of phlogopite across the outcrop gap may be related to the reaction

$$3Do + 1Kfs + 1H_2O \rightleftharpoons 3Cc + 1Phl + 3CO_2 \quad (1)$$

The lowest grade assemblage of the outer aureole is Cc + Do + Tc + Tr + Chl + Mu + Phl and implies the simultaneous equilibria

$$2Tc + 3Cc = 1Tr + 1Do + 1CO_2 + 1H_2O \quad (2)$$

(Fig. 5 upper Tc-field boundary) and

$$49Do + 3Tr + 8Mu + 29H_2O = 8Chl + 8Phl + 55Cc + 43CO_2 \quad (3)$$

(Fig. 6)

Reaction (2) removes talc from the marbles whereas reaction (3) causes muscovite to disappear in the samples under discussion. Very rare quartz-bearing assemblages imply the equilibrium

$$8Qz + 5Do + 1H_2O = 1Tr + 3Cc + 7CO_2 \quad (4)$$

(Fig. 5)

Antigorite occurs together with Do + Cc + Tr.

[2]Abbreviations listed in Table 1a.

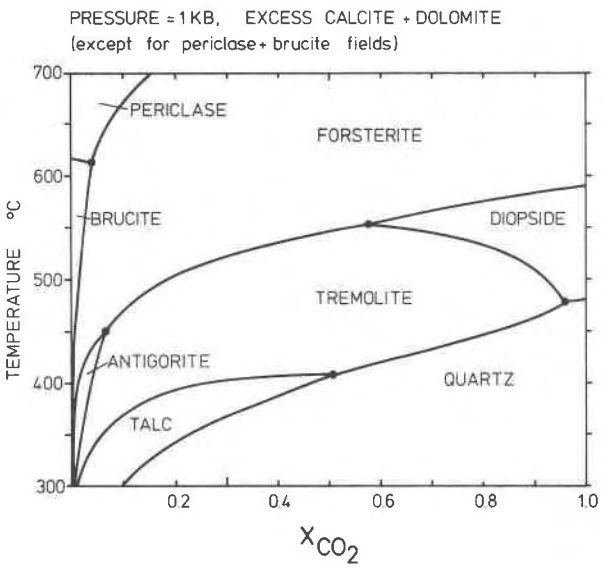

Fig. 5. Isobaric T–X_{CO_2} diagram showing equilibria for siliceous dolomites with excess calcite and dolomite, and the upper stability limits of dolomite at high temperatures and low X_{CO_2}.

This assemblage corresponds to the equilibrium

$$17Tr + 107Do + 107H_2O = 5Ant + 141Cc + 73CO_2. \quad (5)$$

The equilibrium position of this reaction is shown in Figure 5 as the lower boundary of the antigorite field (prograde serpentinization of tremolite). One sample contains forsterite in addition to the four mineral assemblage Cc + Do + Tr + Ant. This five mineral assemblage is confined to the invariant point of Figure 5 terminating the antigorite field towards higher temperatures.

The mineralogical changes at the forsterite–isograd are most adequately described by the reaction

$$1Tr + 11Do \rightleftharpoons 8Fo + 13Cc + 9CO_2 + 1H_2O \quad (6)$$

The equilibrium conditions of this reaction separate the tremolite field from the forsterite field on Figure 5. Aluminium-bearing samples contain spinel and chlorite in addition to Cc + Do + Fo + Tr, indicating that the rocks may have reached conditions which correspond to invariant point (IP2) on Figure 6. The absence of diopside from all rocks of the Cima Uzza profile, furthermore suggests that invariant point (IP2) must be at the water rich side of invariant point (IP3) of Figure 6 and that the X_{CO_2} did not exceed about 0.5 during metamorphism.

The formation of spinel in the Adamello aureole

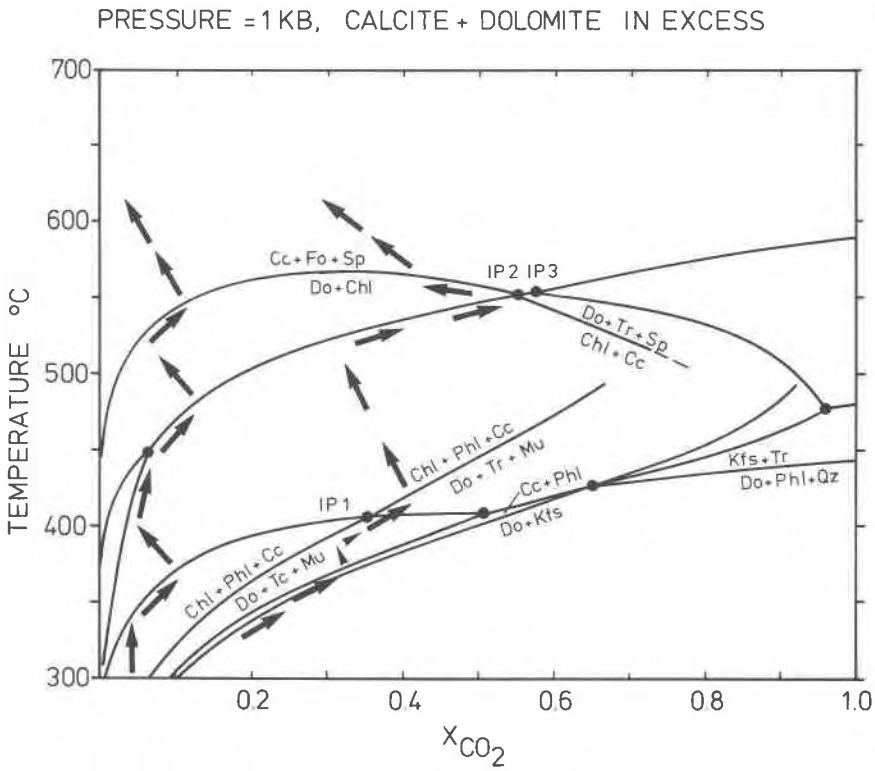

Fig. 6. Isobaric T–X_{CO_2} diagram showing the equilibria for siliceous dolomite as in Fig. 5. In addition, a number of equilibria involving chlorite, spinel, muscovite, phlogopite and K–feldspar are imposed on the system given in Fig. 5. Note: The positions of the equilibria on the CO_2-rich side have not been evaluated. The labeled invariant points are referred to in the text. Two possible paths of metamorphism are given schematically by the arrowed lines.

can be related to the isobaric invariant reaction occurring at invariant point (IP2) (Fig. 6). Excess chlorite was then removed from the rock possibly by the reaction

$$1\text{Chl} + 2\text{Do} \rightleftharpoons 1\text{Sp} + 3\text{Fo} + 2\text{Cc} + 2\text{CO}_2 + 4\text{H}_2\text{O} \quad \text{(Fig. 6).} \qquad (7)$$

The assemblage Do + Cc + Fo + Sp produced by the reactions (6) and (7) remains stable to the innermost part of the aureole and in all samples from the roof pendants. However, as indicated by the occurrence of marbles bearing brucite–pseudomorphs after periclase, the stability conditions for dolomite were apparently exceeded (particularly in the very pure dolomitic marbles) through the reaction

$$1\text{Do} \rightleftharpoons 1\text{Pe} + 1\text{Cc} + 1\text{CO}_2 \text{ (Fig. 5).} \qquad (8)$$

All periclase was subsequently replaced by brucite according to the reaction

$$1\text{Pe} + 1\text{H}_2\text{O} \rightleftharpoons 1\text{Br}. \qquad (9)$$

The observed succession of mineral assemblages in the aureole does not conflict with the interpretation of a progressively metamorphosed sequence along a partially buffered path through the phase diagrams of Figures 5 and 6. The distribution of assemblages as shown on Figures 3 and 4 are fully consistent with the calculated diagrams Figures 5 and 6. The occurrence of talc, antigorite and periclase (as brucite pseudomorphs) suggests that the mineral assemblages coexisted with a relatively H_2O-rich fluid throughout portions of the aureole. As discussed earlier, samples which correspond to the conditions of invariant point (IP2) require fluid compositions with the highest CO_2 content (about 50 mole%). This would indicate that, because most of the reactions from (1) through (8) release CO_2 and tend to drive the fluid compositions towards the CO_2-rich side of the phase diagrams (Figs. 5 and 6), the fluid was diluted with H_2O from an external source while the assemblages travelled through the isobaric divariant fields on Figures 5 and 6. Two possible consistent paths of prograde metamorphism are schematically shown in Figure 6.

In contrast to the profile at Cima Uzza all sam-

ples (Nos. 210–220) from Cima di Agosta are within the forsterite zone. One sample contains the mineral pair diopside + dolomite, indicating higher X_{CO_2} in the metamorphic fluid (Fig. 5). The observed assemblage Di + Do + Cc + Tr + Fo requires conditions of invariant point (IP3) for this sample (Fig. 6). The rock contains spinel in agreement with Figure 6.

Mineral chemistry

The composition of minerals and the distribution of exchangeable elements among them allow for a number of important conclusions on the petrogenesis of these rocks. The analyzed samples are marked with an asterisk on Table 1.

All analyzed ferromagnesian minerals have low, to extremely low iron contents. However, other cations, particularly zinc and vanadium were detected in substantial amounts in spinel. The iron content of minerals from the Cima Uzza profile are also extremely low (*e.g.*, the maximum FeO content of clinohumite is 0.86 wt.%).

Calcite

Calcite is the only mineral whose composition shows a systematic variation across the aureole. The measured calcites are essentially magnesite–calcite solutions. The magnesite component in calcite is buffered by its coexistence with dolomite in all rocks examined. Employing the equation given by Rice (1977) for the temperature dependence of the calcite composition, minimum temperatures of calcite equilibration with dolomite were calculated as shown in Figure 7. The scatter in the calculated temperatures may be attributed to retrograde dolomite exsolution from Mg–calcite. The maximum temperature determined for the roof pendants is in reasonable agreement with estimates given by Jaeger (1957) for the temperature at the immediate contacts of granodiorite or tonalite intrusions. The temperature at the forsterite isograd was found to be near 530°, a value in agreement with the phase diagrams (Figs. 5 and 6). However, the temperature of 500° for the Do + Cc + Tc + Tr sample south of Passo del Frato appears to be distinctly above the upper limit of the talc field (Fig. 5). This discrepancy is partly due to erronously high temperatures calculated from the equation given by Rice (1977) at temperatures below about 550°C (Baumgartner, 1982).

Clinohumite

The compositional characteristics of the analyzed clinohumites are given in Table 2. FeO is uniformly low, most of the samples are low in TiO_2 as well. In contrast the fluorine content is generally high. X_F^{Clh} near the forsterite isograd is typically around 0.6, whereas samples form the roof pendants and the contact show X_F^{Clh} values near 0.4. Clinohumite is always associated with Fo + Cc + Do. These four minerals are related by the equilibrium

$$4Fo + 1Do + 1H_2O = 1Clh + 1CO_2 \quad (10)$$

Equilibrium conditions for the reaction (10) are

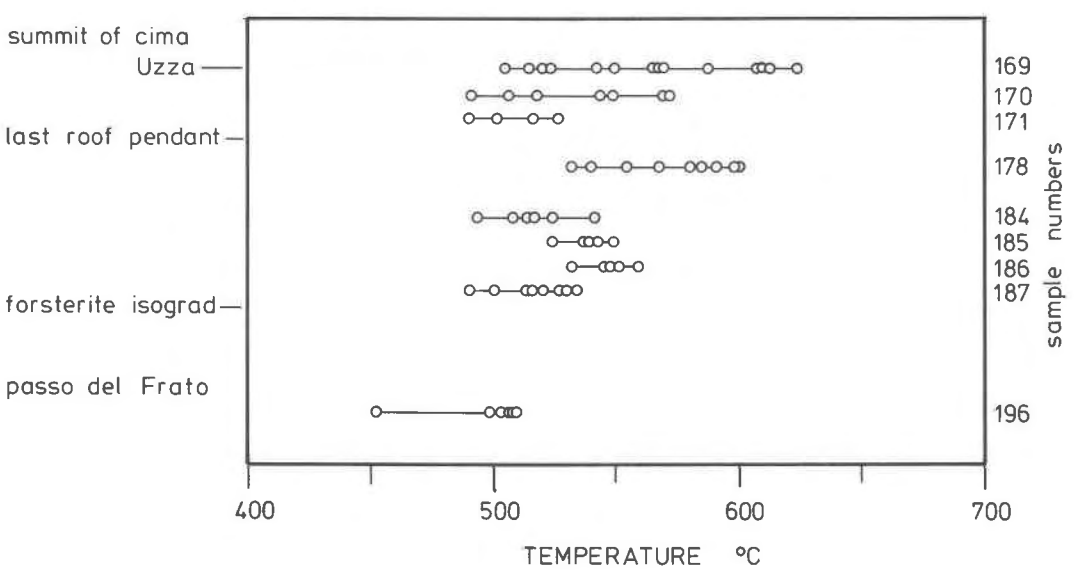

Fig. 7. Temperatures calculated from the composition of Mg–calcite coexisting with dolomite.

Table 2. Microprobe analyses of clinohumite

	185	185	171	178	186	172	170	184	169	189	213
SiO_2	38.51	38.00	38.59	38.02	37.65	38.45	38.47	37.54	38.44	37.70	38.12
TiO_2	-	0.10	0.72	1.64	0.20	1.12	0.85	0.21	-	0.20	1.64
FeO*	0.86	0.44	0.25	0.54	-	0.46	0.65	0.45	0.17	0.55	0.20
MgO	56.25	56.22	56.05	56.64	57.12	56.95	57.47	56.89	58.10	58.65	56.76
H_2O***	1.00	1.20	1.30	1.80	1.10	2.25	1.50	1.20	1.70	2.65	1.20
F	3.70	3.65	3.14	2.60	3.77	1.56	2.55	3.55	2.75	0.67	3.19
Total**	98.80	98.11	98.76	100.17	98.29	100.17	100.42	98.38	100.03	100.14	99.82
Atoms per 18 (O,OH,F)											
Si	4.0591	4.0213	4.0545	3.9445	3.9777	3.9801	3.9927	3.9705	3.9847	3.9117	3.9765
Ti	-	0.0079	0.0568	0.1279	0.0158	0.0871	0.0663	0.0167	-	0.0156	0.1286
Fe	0.0758	0.0389	0.0219	0.0468	-	0.0398	0.0564	0.0398	0.0147	0.0477	0.0174
Mg	8.8375	8.8679	8.7778	8.7588	8.9951	8.7884	8.8875	8.9687	8.9771	9.0706	8.8285
F	1.2334	1.2216	1.0434	0.8531	1.2597	0.5205	0.8370	1.1875	0.9015	0.2198	1.0524
H	0.7031	0.8471	0.9111	1.2457	0.7752	1.5536	1.0384	0.8466	1.1755	1.8341	0.8350
X_F	0.64	0.59	0.53	0.41	0.62	0.25	0.45	0.58	0.43	0.11	0.56

*all Fe as FeO, **total corrected for F. Traces of Ni and Zn. *** stoichimetric H_2O.

presented in Figure 8 for a fluid pressure of 1 kbar and for a number of clinohumite compositions. The equilibria given in this figure have been calculated using the procedure and the thermodynamic data given in Rice (1980) (except for the heat capacity power function coefficient c for magnesite, which is in error in Table 1 (Rice, 1980)). In addition, the variation of the volume change of the solids in the reaction has been taken into account by means of the equation $V_{\text{CLH solid solution}} = X_{\text{F-CLH}}V°_{\text{F-CLH}} + X_{\text{OH-CLH}}V°_{\text{OH-CLH}}$ for each contour of constant clinohumite composition in Figure 8.

The observed compositions of the Adamello clinohumites suggest that the X_{CO_2} at the forsterite isograd was near 0.5 (conditions of point (A) in Fig. 8). This is in agreement with the phase diagram Figure 6.

Marbles from the roof pendants and samples at the contact characteristically coexisted with a more water-rich fluid (X_{CO_2} = 0.1 to 0.4).

Amphibole

The amphibole analyses given in Table 3 can be separated into two chemically distinct groups: (1) Amphiboles from the Agosta profile are essentially pargasites, a composition found by many authors in spinel-bearing dolomites (*e.g.*, Rice, 1977). (2) On the other hand, amphiboles from the Cima Uzza profile are uniformly low in Al and alkalies. No compositional dependence upon the distance from the contact is apparent from the analyses.

Chlorine was found in the forsterite isograd amphiboles in small, but detectable amounts (0.1–0.2 wt.% Cl).

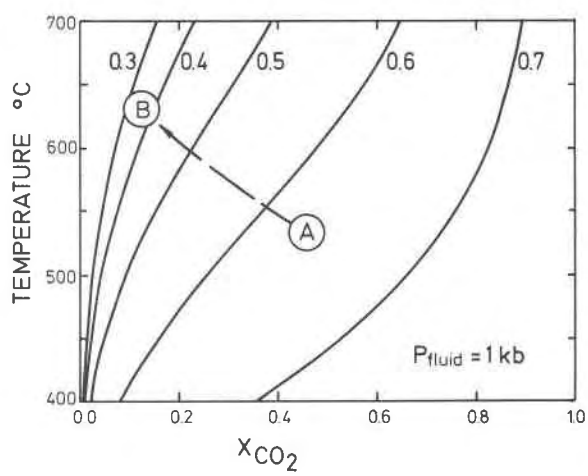

Fig. 8. Isobaric temperature versus X_{CO_2} diagram showing the equilibrium conditions for the reaction 4Fo + 1Do + $1H_2O$ = 1Clh + $1CO_2$ for different compositions of clinohumite (contours for X_{F-Clh}).

Table 3. Microprobe analyses of amphibole

	186	189	169	185	211	210
SiO_2	55.02	58.80	57.81	58.11	46.55	44.27
TiO_2	-	0.13	0.23	-	0.52	1.33
Al_2O_3	3.77	0.20	1.43	1.35	13.95	15.40
FeO	0.20	0.13	0.41	0.29	1.30	1.07
MgO	23.11	25.20	24.03	23.67	19.24	18.85
CaO	12.84	12.47	13.44	13.55	13.15	13.14
Na_2O	0.94	1.13	0.23	0.13	2.01	2.53
K_2O	0.16	0.16	0.05	-	0.47	0.66
F	0.65	0.42	0.18	0.27	0.40	0.49
Total*	98.58	100.47	99.73	99.43	99.98	99.71
* Total corrected for F, including 2% H_2O and traces of V,Zn,Cl						
Atoms per 24 (O,OH,F)						
Si	7.5897	7.9402	7.9713	7.9237	6.4773	6.1908
Ti	-	0.0132	0.0235	-	0.0544	0.1398
Al	0.6129	0.0318	0.2294	0.2169	2.2877	2.5381
Fe	0.023	0.0146	0.0466	0.0330	0.1512	0.1251
Mg	4.7517	5.0722	4.8768	4.8108	3.9905	3.9291
Ca	1.8962	1.8042	1.9607	1.9796	1.9605	1.9688
Na	0.2514	0.2958	0.0607	0.0343	0.5422	0.6859
K	0.0381	0.0275	0.0086	-	0.0834	0.1177
F	0.2835	0.1836	0.0775	0.1164	0.1760	0.2167

Sheet silicates

Sheet silicate analyses are given in Table 4.

Phlogopite. Phlogopite analyses show a correlation between composition and distance from the contact. Parallel to the inferred direction of temperature increase, an enrichment in aluminium and a corresponding decrease in silica was detected.

Chlorite. The total Al per 36 anions varies between 4.52 and 4.88 (excluding sample 184, possibly late chlorite). This variation cannot be related to the inferred temperature distribution in the aureole. The observed excess Al of 0.52 to 0.88 (relative to stoichiometric clinochlore) suggests that the analyzed chlorite in fact represents chlorite in chemical equilibrium with the remaining minerals at the determined temperatures between 500–550° (Widmark, 1980).

Oxides and sulfides

Spinel. The chemical analyses of spinel, given in Table 5, show remarkable variation. All samples (except 216) are very low in iron, however, they may contain as much as 2.5 wt.% V_2O_3 (single spot analyses revealed maximum wt.% V_2O_3 near 4.00, and indicated an inhomogeneous distribution of vanadium in spinel). The spinels with the highest vanadium contents were found in the roof pendants near the summit of Cima Uzza. Spinels from near the forsterite isograd are remarkably rich in zinc. Spinel with about 7% gahnite-component was found in sample 184. From the same locality, in sample 185, abundant sphalerite was detected. The curious compositional variations found in spinel are likely to reflect local variations in fluid-composition. The heavy metal content of this fluid may be derived from the pluton itself. The occurrence of particularly gahnite-rich spinel and sphalerite is restricted to the forsterite isograd.

Other oxides and sulfides. The observed oxides in the microprobe samples include magnetite, ilmenite and rutile (Table 1). Of the sulfides, pyrrhotite is the most abundant. In some samples pyrite is also present. Galena occurs in some samples, for instance in the assemblage galena–sphalerite–pyrite. Pentlandite was found in one marble sample together with pyrite. This nickel mineral most probably was precipitated from fluids derived from the pluton. It was found that sphalerite contains about 7 mole% FeS, ilmenite has about 1.6 wt.% MnO and 4% V_2O_3, pyrrothite typically contains up to 1% wt.% NiO, while rutile contained as much as 8 wt.% vanadium expressed as V_2O_5. The composition of pentlandite is 46 wt.% NiS and 53% FeS.

Petrographic observations

In the nodular marble the nodules are dramatically enriched in silicates and oxide minerals in the forsterite zone. Figure 9a shows the assemblage Fo + Sp + Chl in a pure calcite matrix. Note the remarkable modal abundance of all minerals relative to calcite.

Even more pronounced are the textural relations of sample 172 (Fig. 9b). The assemblage is Cc + Do + Fo + Sp + Clh. The modal abundance of Fo + Sp + Clh exceeds 60% in this sample. However, there is still some modal dolomite present. This observation suggests that the assemblage Fo + Sp + Clh in this rock is unlikely to be the result of an isochemical metamorphism of an originally sedimentary silicious dolomite (maximum Fo-content of "siliceous dolomite" cannot exceed 38 vol.% Fo (Bucher, 1981a).

It may still be argued that the observed concentrations of silicate and oxide minerals in the nodules might be the result of a redistribution of chemical species on a small scale only. The silicate nodules could then represent metamorphic segregations.

Table 4. Microprobe analyses of sheet silicates

	Phlogopite			Muscovite	Talc	Chlorite				
	187	196	216	196	196	185	187	196	178	184
SiO_2	39.48	43.17	36.85	47.25	61.89	30.02	31.19	30.37	29.96	32.30
TiO_2	1.00	0.41	1.01	0.16	0.0	-	-	-	-	-
Al_2O_3	16.00	14.63	18.96	29.88	0.25	20.61	20.37	21.84	21.82	19.70
FeO	0.10	0.68	2.40	4.00	0.53	0.44	0.37	1.43	0.53	0.37
MgO	25.31	25.29	25.78	1.77	32.23	36.96	34.75	34.15	34.15	34.65
K_2O	10.01	9.95	9.51	11.36	-	-	-	-	-	-
H_2O*	4.0	4.0	4.2	4.0	4.15	12.20	12.20	12.20	12.20	12.20
F	0.83	1.07	0.04	0.10	0.29	-	-	-	-	-
sum**	96.98	98.76	98.73	98.67	99.56	100.23	98.88	100.59	98.67	99.21
	atoms per 24 (O,OH,F)					atoms per 36 (O,OH,F)				
Si	5.6179	6.0074	5.2235	6.4814	7.8978	5.6104	5.8729	5.6639	5.6605	6.0539
Ti	0.1070	0.0429	0.1076	0.0165	0.0047	-	-	-	-	-
Al	2.7840	2.3994	3.1676	4.8307	0.0375	4.5397	4.5205	4.8004	4.8588	4.3517
Fe	0.0119	0.0791	0.2845	0.4588	0.0554	0.0687	0.0582	0.2230	0.0853	0.0579
Mg	5.3683	5.2456	5.4470	0.3618	6.1303	10.2959	9.7530	9.6598	9.6172	9.6800
K	1.8171	1.7663	1.7197	1.9878	-	-	-	-	-	-
H	3.7968	3.7130	3.9713	3.8431	3.7879	15.2093	15.3237	15.1772	15.3758	15.2529
F	0.3735	0.4705	0.0179	0.0433	0.1180	-	-	-	-	-

* stoichiometric H_2O, ** sum corrected for F. Traces of V,Zn,Cr,Ni and Na.

However, the unmetamorphosed dolomites and the tremolite-zone marbles contain very small portions of noncarbonate minerals. An extremely large volume of marble would have to be depleted in silicate minerals in order to form the observed concentrations in the nodules. In addition, the matrix dolomite of the forsterite zone samples is very similar in bulk rock composition to the tremolite zone marbles and the unmetamorphosed dolomite (*i.e.*, very low in silicate minerals) (Callegary, 1962). It is necessary to again stress that cherty nodules were not found in the unmetamorphic source rock.

In sample 171, domains containing swarms of small Fo + Clh + Sp grains in a pure dolomite matrix can be observed. In many other samples modal forsterite exceeds 50%, in sample 181 some domains with modal spinel exceeding 50% (in pure carbonate matrix) have been observed. In sample 178, in the nodule domains, the sum of modal carbonate may be as low as 10%, however, the carbonate is still calcite and dolomite. Another striking feature of the forsterite zone samples is the frequent occurrence of very closely spaced and dense fluid and solid inclusion trails which cut through all minerals in a given assemblage (Fig. 9c). The absence of alteration products such as chlorite and serpentine along these solid + fluid inclusion trails suggests that they are probably related to the formation of the high grade assemblage. It is thought that these inclusion trails represent healed microcracks. A very unusual growth texture in olivine was observed in some samples, particularly 180 (Fig. 9d). In these rocks, irregular cloudy areas may be recognized in olivine. Frequently these brownish cloudy fields occupy the core regions of an olivine grain and are overgrown by rims of clear olivine. The cloudy volume of the olivine is composed of a very dense cloud of fluid inclusion bubbles and the texture is comparable to that of pumice or sponge. The texture may be the result of very rapid olivine growth under the conditions of an extraordinarily high fluid/rock-ratio.

Discussion of a model for the aureole formation

The observations and mineral compositional data presented in the proceeding sections strongly suggest that the mineral assemblages formed by reaction of a SiO_2-rich fluid with pure dolomite. This

Table 5. Microprobe analyses of spinel

	178	172	170	184	213	211	216	171	187	186	214
TiO_2	0.14	0.99	0.50	0.28	0.20	0.00	0.32	0.59	0.08	0.00	0.00
Al_2O_3	69.99	66.55	66.00	69.01	69.35	69.78	63.47	67.18	70.57	70.71	69.46
V_2O_3	0.64	2.53	2.48	9.17	1.55	0.00	0.14	2.26	0.09	0.21	0.96
Cr_2O_3	0.00	0.21	0.38	0.08	0.12	0.00	0.17	0.17	0.08	0.00	0.11
ZnO	0.35	0.27	0.30	3.85	1.30	0.79	0.34	0.36	0.73	0.86	1.55
FeO*	2.92	1.81	2.54	0.82	0.38	3.88	11.37	1.52	1.06	1.18	0.36
MgO	26.87	27.43	27.17	24.84	26.37	24.64	23.42	27.17	26.79	27.37	26.65
Total**	100.90	99.86	99.47	99.04	99.27	99.18	99.24	99.35	99.48	100.50	99.60
Number of cations per 4 oxygens											
Ti	0.0025	0.0179	0.0092	0.0052	0.0035	0.0000	0.0061	0.0107	0.0014	0.0000	0.0000
Al	1.9694	1.8984	1.8996	1.9914	1.9705	2.0035	1.8931	1.9057	1.9950	1.9828	1.9717
V	0.0126	0.0491	0.0485	0.0030	0.0300	0.0000	0.0029	0.0438	0.0010	0.0038	0.0187
Cr	0.0000	0.0040	0.0073	0.0015	0.0022	0.0000	0.0034	0.0030	0.0015	0.0000	0.0020
Zn	0.0060	0.0049	0.0053	0.0696	0.0200	0.0141	0.0063	0.0064	0.0129	0.0151	0.0275
Fe	0.0583	0.0367	0.0519	0.0168	0.0076	0.0791	0.2406	0.0307	0.0212	0.0243	0.0072
Mg	0.9562	0.9894	0.8900	0.9062	0.9476	0.8948	0.8848	0.9802	0.9578	0.9706	0.9567

* all Fe expressed as FeO, ** total includes traces of Ni.

conclusion is further sustained by the observed dependence of the total rock composition on the distance to the contact. A dramatic increase in the modal abundance of non-carbonates is recognized at the forsterite isograd. This observation implies that the forsterite isograd represents, not only the reaction isograd $1Tr + 11Do \rightleftharpoons 8Fo + 13Cc + 9CO_2 + 1H_2O$, but also appears to be the trace of a metasomatic front surface. This metasomatic front can most adequately be characterized by the reaction $2Do + 1SiO_{2aq} \rightleftharpoons 1Fo + 2Cc + 2CO_2$. The forsterite isograd is not isochemical. The observed increase of modal silicate minerals across the forsterite isograd may be as large as 10 fold.

Figure 10 shows 5 different paths of bulk chemistry modification as deduced from the microtextures. The reaction along the paths can be written as

$$2Do + SiO_{2aq} \rightleftharpoons Fo + 2CO_2 + 2Cc. \quad (11)$$

If CaO is conserved in the reaction, a Fo + Cc + Do rock of composition (A) results, or if dolomite is totally consumed by the reaction a Fo–Cc-rock of composition (B) will be the end product. Many of the local textures suggest, however, that CaO was not conserved during the reaction but was rather removed from the rock, resulting in extremely forsterite-rich areas (path C + D). The extreme case of swarms of forsterite grains in a pure dolomite matrix may be represented by path (E) and the corresponding reaction is:

$$2Do + SiO_{2aq} + 4\,HCl \rightleftharpoons Fo + 2CO_2 + 2CaCl_2 + 2H_2O \quad (12)$$

or in ionic form

$$2Do + SiO_{2aq} + 4H^+ \rightleftharpoons Fo + 2CO_2 + H_2O + 2Ca^{++}.$$

Reaction paths A and B characterize the forsterite isograd, whereas with decreasing distance to the contact, loss of CaO becomes increasingly important. Paths D or E are characteristic of nodular marbles from the roof pendants.

In Figure 11, a model for SiO_2-metasomatism in dolomitic marbles is presented for 1 kbar pressure. The occurrence of talc, serpentine and brucite, together with the absence of diopside and the composition of clinohumite suggests that X_{CO_2} was low throughout. The activity of H_2O was held constant at a value of 0.5. This corresponds to the presumed conditions existing at the forsterite isograd and the invariant point IP2 of Figure 6. For the rocks in the Cima Uzza aureole this represents the

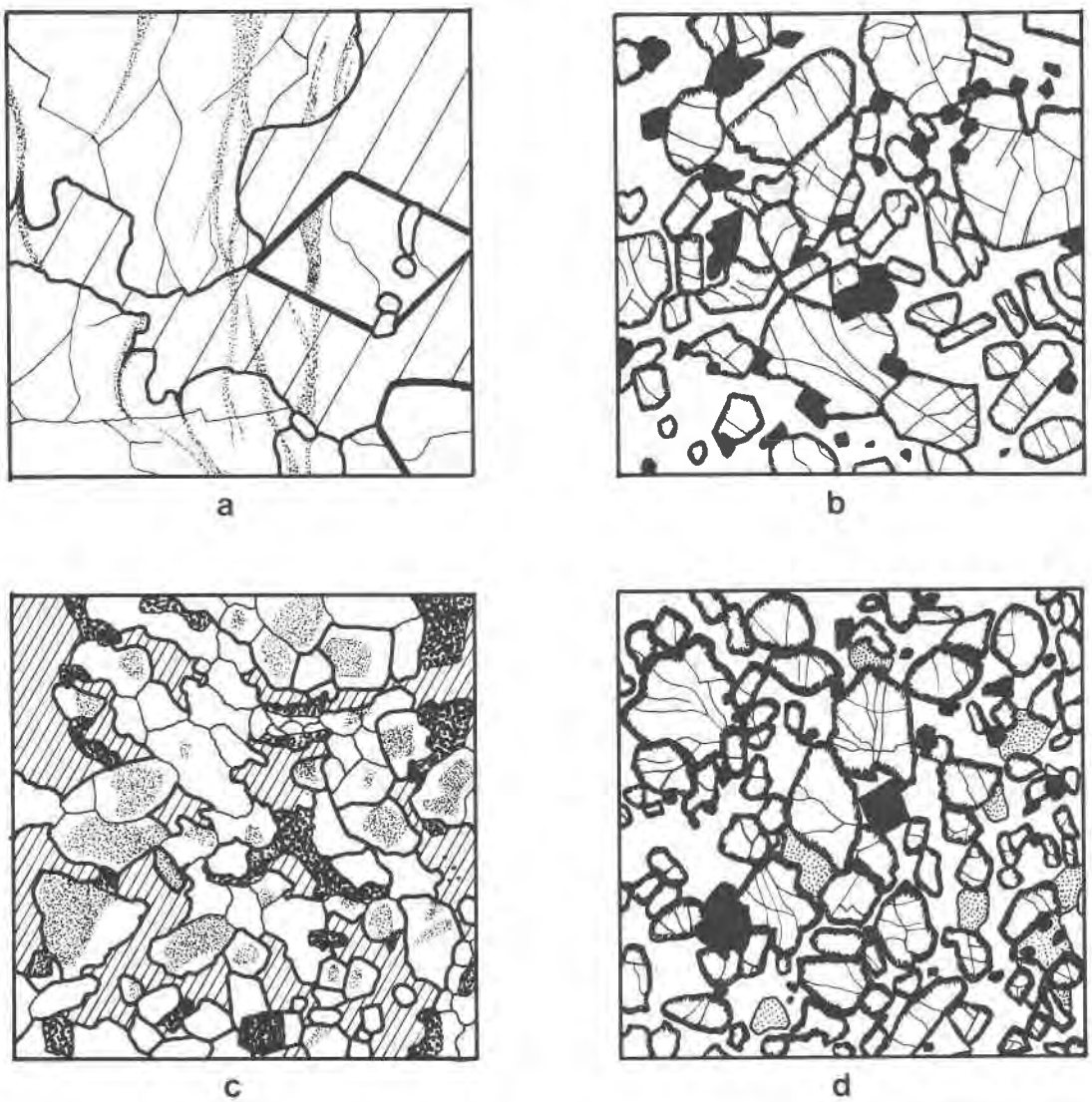

Fig. 9. Microtextures of samples from the forsterite zone (figures drawn from photomicrographs, the frame of the drawings measures 2 × 2 mm). (a) Sample 181: Assemblage calcite (white) + forsterite (irregular cleavage) + spinel (black). Forsterite slightly elongated parallel to *c*. (b) Sample 172: Assemblage calcite (white) + dolomite (stipled) + forsterite (irregular cleavage) + clinohumite (not distinguished from forsterite) + spinel (black). (c) Sample 176: Assemblage calcite (dashed) + forsterite (irregular cleavage) + clinohumite (not distinguished from forsterite) + spinel (euhedral crystal). Note the entrainment of solid and fluid inclusions (stipled) cutting across the minerals of the assemblage. (d) Sample 180: Assemblage carbonate (dashed) + forsterite (white) + spinel (black). Note the irregular cloudy areas in forsterite, partly with clear forsterite overgrowths. Spinel in this sample occurs also as clustered aggregates of very small grains.

lower limit for the activity of water which was probably much higher for most other portions of the aureole. The activity of water was chosen to be 0.5 in Figures 11 and 12 in order to be consistent with the observed coincidence of the forsterite and spinel isograd. Under these given constraints and with calcite in excess, the equilibrium conditions of reactions such as reaction (11) can be shown in terms of $a_{SiO_{2aq}}/\sigma_{SiO_{2aq}}$ and temperature. A SiO_2-rich fluid lost from the pluton will tend to drive the fluid composition in the dolomitic marble rapidly towards the reaction boundary of the dolomite–forsterite reaction when passing through cracks and open pore space in the marble. The continued precipitation of forsterite subsequently buffered the fluid composition along the dolomite–forsterite field

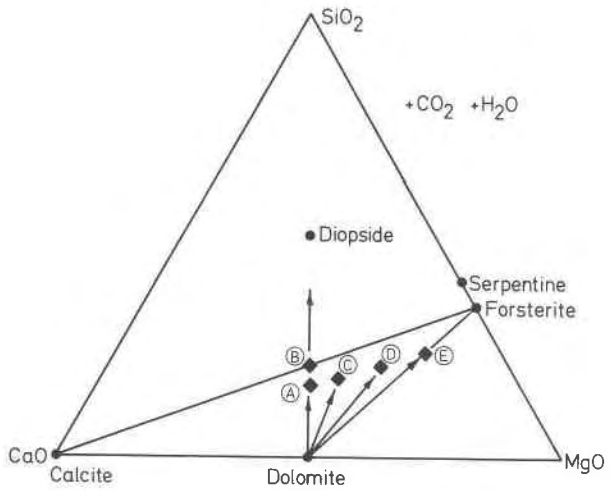

Fig. 10. Path of bulk chemistry alteration by SiO_2-metasomatism as inferred from local microtextures (Fig. 9).

boundary (Fig. 11). This filtration mechanism would effectively absorb dissolved SiO_2 from the fluid. The filtration path is essentially given by the equilibria involving dolomite (arrow path Fig. 11). The most significant mass transfer occurred along the dolomite–forsterite-boundary at high temperatures and in rocks close to the pluton. SiO_2-rich fluid, upon reaching the outer aureole, could precipitate tremolite, or in the low-temperature regime, talc or quartz, and provided X_{CO_2} was low enough, antigorite (not present under the conditions of Fig. 11). Although much of the tremolite of the tremolite-zone of the outer aureole such as vein-tremolite or tremolite coatings of open pore space could have formed by such a filtration mechanism, some of the tremolite must be attributed to tremolite-formation from Qz + Do initially present in the rocks.

With this interpretation of the aureole, the forsterite isograd is equivalent to the outer limit of an infiltration front. SiO_2-metasomatism beyond this front was apparently restricted to highly permeable fractures or very porous rocks. In addition, the minor modal tremolite found in the tremolite-zone of the aureole could be explained by the decreasing likelihood that a SiO_2-rich solution would have been able to reach the outer aureole. As shown in Figure 11 the precipitation of tremolite requires a fluid with $a_{SiO_{2aq}}/\sigma_{SiO_{2aq}}$ 100 times higher than what is required for forsterite production in the vicinity of the contact. Most of the SiO_{2aq} given off by the pluton is therefore expected to be filtered out of the fluid in the forsterite zone of the inner aureole.

The inferred aluminium metasomatism may be modeled in an analogous manner to the SiO_2-metasomatism (Fig. 12). Spinel-precipitation will filter most of the aluminium out of a fluid introduced to the marbles from the pluton along a path section (A). This occurs within the forsterite zone. The observed coincidence of the forsterite isograd with the first and abundant occurrence of spinel further supports the interpretation that the two mineralogical boundaries which appear to coincide in the field represent an infiltration front. Along path section (B) (Fig. 12) chlorite is expected to form from Al-metasomatism in the outer portion of the forsterite-zone. This zone, characterized by the assemblage Do + Fo + Cc + Chl is very narrow, if present at all in the Cima Uzza profile. In the outer aureole, chlorite may be formed along path (C) and result in the observed characteristic assemblage Cc + Do + Tr + Chl. Comments made on tremolite-formation by SiO_2-metasomatism apply in an analogous way to chlorite formation.

Summary and conclusions

The mineralogical and rock-compositional zonation observed in dolomites in the contact aureole may have formed by silica- and aluminium metasomatism. This conclusion was deduced from microtextural characteristics and observed modal variations in the rocks, as well as from textures on the scale of hand specimens, and the composition of the minerals (*e.g.*, clinohumite).

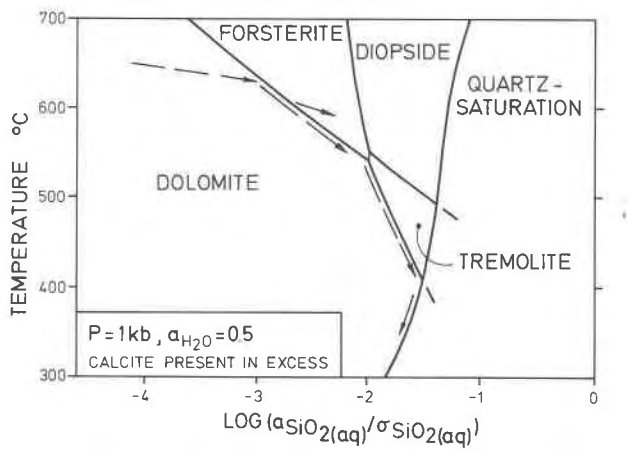

Fig. 11. Isobaric temperature *vs.* log $(a_{SiO_{2aq}}/\sigma_{SiO_{2aq}})$ diagram at constant a_{H_2O}. The path of SiO_2 infiltration along the dolomite field boundary is given schematically by dashed arrows. The arrow inside the divariant forsterite + calcite field shows a rarely realized path in the forsterite zone. For this case, dolomite is totally consumed by the metasomatic rection. The conditions necessary for the forsterite–diopside reaction apparently did not occur in the samples examined.

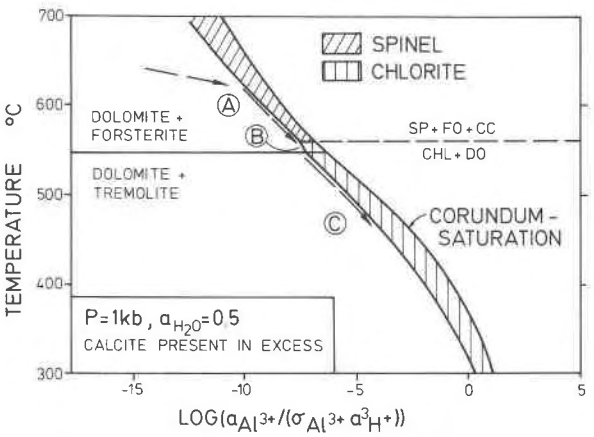

Fig. 12. Isobaric temperature *vs.* log ($a_{Al^{3+}}/\sigma_{Al^{3+}} \cdot a^3_{H^+}$) diagram at constant a_{H_2O}. Infiltration path of Al-metasomatism shown by dashed arrows. In the upper portion (>540°) of the diagram, calcite + forsterite are stable, below this temperature tremolite + calcite are present in excess.

The field observations suggest that the metasomatic infiltration front did not advance through the bulk volume of the dolomite, but that fluid flow was focused by the interconnected cavity space in the dolomite. The infiltration front is manifested as a mapable boundary in the field and characterized by the first and abundant appearance of forsterite. However, minor evidence of metasomatism can be found in the outer aureole as well (tremolite-coatings, antigorite-veins). The absence of diopside, the occurrence of talc, antigorite, brucite and the composition of clinohumite indicate that a_{H_2O} was above about 0.7 throughout the aureole except for rocks at the forsterite isograd, where it probably was as low as 0.5.

The coincidence of the spinel and forsterite isograds is likely to be the result of a homogeneous source fluid composition from the large reservoir of igneous rocks. The source fluid reacting with the dolomitic country rocks was initially in equilibrium (or nearly so) with the source tonalite.

It is conceivable, that metasomatic aureole formation was imposed on a sequence of initially isochemical prograde metamorphism of low-silica dolomite, below the maximum temperature conditions. This could at least partly explain the apparent discrepancies between the Cc–Do temperatures from the outer aureole and the calculated phase diagrams.

Acknowledgments

I thank Ian Hutcheon and Jack Rice for their critical reviews which substantially improved this contribution. I am indebted to Volkmar Trommsdorff and Ezio Callegari for valuable discussions about various aspects of the geology of the Adamello area. Martin Frey kindly supported the study by introducing the author to the analytical techniques necessary for dealing with very fine-grained, low grade carbonate rocks. Assistance during the field work by Heiko Oterdoom and Roli Oberhänsli is gratefully acknowledged. I thank Susanne Tobler for typing various versions of this manuscript. The field work and a part of the laboratory work was supported by the Schweizerischer Nationalfonds, grant 2.615-0.75 (Prof. V. Trommsdorff, ETH, Zurich, Switzerland).

References

Bianchi, A. and Dal Piaz, A. G. (1948) Differenziazioni petrografiche e metamorfismi selettivi di contatto nel Massiccio dell'Adamello. Rendiconti della Società Italiana di Mineralogia e Petrologia, 5, 3–26.

Baumgartner, L. (1982) Petrographische Untersuchungen auf der Alp Confin (Mesocco, Graubünden). Ms. Thesis. Universität Basel.

Bucher-Nurminen, K. (1981a) The formation of metasomatic reaction veins in dolomitic marble roof pendants in the Bergell intrusion (Province Sondrio, Northern Italy). American Journal of Science, 281, 1197–1222.

Bucher-Nurminen, K. (1981b) Petrology of chlorite–spinel marbles from northwestern Spitsbergen (Svalbard). Lithos, 14, 203–213.

Callegari, E. (1962) La Cima Uzza (Adamello Sud-Orientale). Parte I. Studio petrografico e petrogenetico delle formazioni metamorfiche d contatto. Memorie degli Istituti di Geologia e Mineralogia dell' Università di Padova, 23, 116.

Carpenter, A. B. (1967) Mineralogy and petrology of the system CaO–MgO–CO_2–H_2O at Crestmore, California. American Mineralogist, 52, 1341–1363.

Fawcett, J. J. and Yoder, H. J., Jr. (1966) Phase relations of chlorites in the system MgO–Al_2O_3–SiO_2–H_2O. American Mineralogist, 51, 353–380.

Finger, L. W. and Burt, D. M. (1971) Reaction, a FORTRAN IV computer program to balance chemical reactions. Carnegie Intitution of Washington, Year Book, 71, 617–620.

Flowers, G. (1978) FINDX: Computer program library, theoretical geochemistry, H. C. Helgeson. University of California, Berkeley.

Greenwood, H. J. (1975) Buffering of pore fluids by metamorphic reactions. American Journal of Science, 275, 573–594.

Helgeson, H. C., Delany, J. M., Nesbitt, H. W. and Bird, D. K. (1978) Summary and critique of the thermodynamic properties of rock-forming minerals. American Journal of Science, 278–A.

Jaeger, J. C. (1957) The temperature in the neighborhood of a cooling intrusive sheet. American Journal of Science, 255, 306–318.

Kerrick, D. M. (1970) Contact metamorphism in some areas of The Sierra Nevada, California. Geological Society of America Bulletin, 81, 2913–2938.

Masch, L. (1977) Die Aureole des Monzoni-Intrusivkomplexes (Norditalien)—ein Modell progressiver Thermometamorphose kieseliger Karbonate. Habilitationsschrift, Universität München.

Melson, W. G. (1966) Phase equilibria in calc–silicate hornfels, Lewis and Clark County, Montana. American Mineralogist, 51, 402–421.

Moore, J. W. and Kerrick, D. M. (1976) Equilibria in siliceous dolomites of the Alta Aureole, Utah. American Journal of Science, 276, 502–524.

Rice, J. M. (1977) Contact metamorphism of impure dolomitic limestone in the Boulder Aureole, Montana. Contributions to Mineralogy and Petrology, 59, 237–259.

Rice, J. M. (1980) Phase equilibria involving humite minerals in impure dolomitic limestone. Part I: Calculated stability of clinohumite. Contributions to Mineralogy and Petrology, 71, 219–235.

Suzuki, K. (1977) Local equilibrium during the contact metamorphism of siliceous dolomites in Kasuga-mura, Gitu-ken, Japan. Contributions to Mineralogy and Petrology, 61, 79–89.

Taylor, B. E. and O'Neil, J. R. (1977) Stable isotope studies of metasomatic Ca–Fe–Al–Si skarns and associated metamorphic and igneous rocks, Osgood Mountains, Nevada. Contributions to Mineralogy and Petrology, 63, 1–49.

Tromsdorff, V., and Evans, B. W. (1977) Antigorite–ophicarbonates: phase relations in a portion of the system CaO–MgO–SiO_2–H_2O–CO_2. Contributions to Mineralogy and Petrology, 60, 39–56.

Walther, J. V. and Helgeson, H. C. (1977) Calculation of the thermodynamic properties of aqueous silica and the solubility of quartz and its polymorphs at high pressures and temperatures. American Journal of Science, 277, 1315–1315.

Walther, J. V. and Helgeson, H. C. (1980) Description and interpretation of metasomatic phase relations at high pressures and temperature. I. Equilibrium activities of ionic species in non-ideal mixtures of CO_2 and H_2O. American Journal of Science, 280, 575–606.

Widmark, T. (1980) The reaction chlorite + dolomite = spinel + forsterite + calcite + carbon dioxide + water. Contributions to Mineralogy and Petrology, 72, 175–179.

Manuscript received, June 30, 1981;
accepted for publication, June 17, 1982.